

Multi-Band Circularly Polarized Ferrite Antenna Operating with Negative Effective Permeability

J. Leon Valdes, T. Monédière, E. Arnaud, S. Jemmeli, and L. Huitema

Abstract—This paper presents the development of an antenna device operating with a right-hand circular polarization (RHCP) for Global Navigation Satellite Systems (GNSS) applications, operating in the frequency bands L1 (1.5756 GHz), L2 (1.227 GHz) and E6 (1.278 GHz). The antenna exploits the potential of biased ferrite materials to naturally generate a circular polarization. In addition, to achieve a right-hand circular polarization over a wide frequency band, the antenna uses a carefully selected and polarized ferrite material to ensure that the device operates where the effective permeability of the ferrite has a negative real part. It also allows the reduction of antenna dimensions due to the high permittivity of ferrites. All performances in terms of impedance matching and radiation pattern are reported and the concept is validated by the prototype measurements.

Index Terms—Circular polarization, ferrite materials, multi-band antenna, negative effective permeability.

I. INTRODUCTION

CURRENTLY there is a growing need to develop more compact antennas that can operate on several frequency bands for multi-standard wireless communication systems. In addition, circular polarization radiation provides a valuable solution in various fields. It overcomes misalignments between transmitters and receivers, mitigates the effects of deflections, propagation and ground reflections in satellite applications and reduces polarization losses caused by multipaths [1]. The technical challenge of this work is to combine compactness, circular polarization radiation and multi-band operation in the same device.

In order to obtain circular polarization within an antenna, a classical technique consists of using a feeding line (single or multiple) to excite two orthogonal linearly polarized modes with a phase difference of 90° [2], [3]. Other techniques rely on the integration of disturbance zones on the antenna [1], [4], [5], [6].

These approaches can enable dual-band operation, but often present constraints in terms of bandwidth and size [7], [8]. Interesting antennas in terms of bandwidth and axial ratio have been proposed, but feeding them through a coupler increases

the footprint and losses [9]. Other papers have focused on broadband designs, but have also encountered size limitations [10], [11]. Finally, a method based on spherical mode development shows an antenna operating on the L1 and L2 bands by using an antenna array loaded by optimized impedances, the array remains miniature while exhibiting satisfactory performance [12].

A good alternative is to develop ferrite-based antennas because these materials, when polarized by a continuous (DC) magnetic field, exhibit specific properties, including anisotropy and non-reciprocal behavior, which enable circularly polarized waves (RHCP and LHCP) to be generated naturally [13], [14], [15], [16]. In addition, their permeability often greater than 1 associated with a high permittivity (typically between 12 and 16), make ferrites ideal substrates for the miniaturization of antennas [17], [18].

Notably, previous works [19], [20], [21], [22], [23] have proven that a ferrite-based patch antenna could generate good quality circular polarization while being miniature. Based on this work, ferrite materials show great potential for meeting the challenges of compactness, multi-band operation and circular polarization. However, a few drawbacks stand out:

- It is not possible to select operating frequencies independently of each other [18].
- When multi-band, the circular polarization generated changes (right or left) depending on the mode excited (TM_{-11} or TM_{+11})
- Impedance matching bandwidths are too low to be compatible with GNSS applications

These three points are linked to the fact that these proposed antennas operate in particular zones for ferrite material. Indeed, ferrite permeability parameters depend on frequency and DC magnetic field, enabling ferrite devices to be operated in different zones. Working in both zones at the same time was demonstrated in [24], revealing that an antenna can operate on three different (non-independent) frequency bands while radiating RHCP and LHCP polarizations simultaneously. These three frequencies correspond to the natural modes of the ferrite, governed by the internal static magnetic field and the radius of

¹This paragraph of the first footnote will contain the date on which you submitted your paper for review.

T. Monédière is with XLIM Research Institute, University of Limoges, 87000, FR (e-mail: thierry.monediere@unilim.fr).

E. Arnaud is with XLIM Research Institute, University of Limoges, 87000, FR (e-mail: eric.arnaud@unilim.fr).

S. Jemmeli was with XLIM Research Institute, University of Limoges, 87000, FR. She is now with Exens-solutions, Les Ulis, Île-de-France 91940, FR (e-mail: sarra.jemmeli@exens-solutions.com).

L. Huitema is with XLIM Research Institute, University of Limoges, 87000, FR and with the Institut Universitaire de France (IUF), (e-mail: laure.huitema@unilim.fr).

Corresponding author: J. Leon Valdes is with XLIM Research Institute, University of Limoges, 87000, FR (e-mail: jehison.leon-valdes@unilim.fr).

the ferrite resonator.

In this paper, a tri-band circularly polarized antenna is developed using a ferrite material operating in a region where the real part of the effective permeability (μ_{eff}) is negative. In this region, only one mode (the natural mode of the ferrite) is excited to produce a single type of circular polarization. The device is excited by a single microstrip line, and the patch is etched on a single ferrite substrate magnetized by a permanent magnet. It operates in the L1 (1.5756 GHz), L2 (1.227 GHz) and E6 (1.278 GHz) frequency bands for GPS and Galileo applications, and features RHCP radiation at all operating frequencies. These frequencies are achieved through a matching circuit in the feeding line and an etched slot on the patch. The paper is divided in five main sections.

Section II is dedicated to the presentation of the most significant parameters of ferrites, i.e. its permeability tensor and the effective permeability.

Section III is dedicated to the modal study of a ferrite cavity while focusing on the domain where the real part of the effective permeability is negative.

Section IV is an electromagnetic validation of the modal study presented in Section III. This section will show that the resonator antenna has a good circular polarization on a wide frequency band without being matched on the whole frequency band. An impedance matching circuit is implemented to enable the antenna to operate on the three frequency bands L1, L2 and E6. This section will first consider the antenna modeled in an ideal case, i.e. when the magnetic field inside the ferrite substrate is homogeneous and then in a real case when the inhomogeneous applied magnetic field is provided by a permanent magnet with a magnetostatic/electromagnetic co-simulation.

Finally, Section V will present the prototyping of such an antenna, with experimental performances discussed and compared with the state of the art.

II. FERRITE SUBSTRATE CHARACTERISTICS

The anisotropic and non-reciprocal behavior of saturated ferrites under a DC biasing magnetic field is characterized by their permeability tensor, also known as the Polder tensor (1) [17], [25]:

$$[\mu_r(\omega)] = \begin{bmatrix} \mu & -j\kappa & 0 \\ j\kappa & \mu & 0 \\ 0 & 0 & 1 \end{bmatrix} \quad (1)$$

Where the Polder tensor elements are given by:

$$\begin{aligned} \mu &= 1 + \frac{\omega_m(\omega_0 + j\omega\alpha)}{(\omega_0 + j\omega\alpha)^2 - \omega^2} = \mu' - j\mu'' \\ \kappa &= \frac{\omega_m\omega}{(\omega_0 + j\omega\alpha)^2 - \omega^2} = \kappa' - j\kappa'' \end{aligned} \quad (2)$$

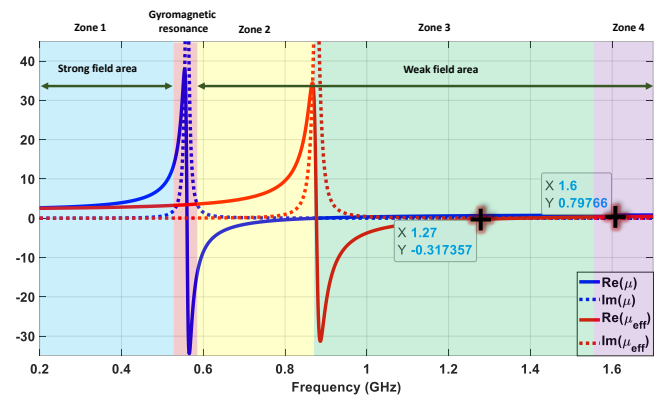
With: $\omega = 2\pi f$, ω_m is the gyrotropic angular frequency defined by $\omega_m = \gamma\mu_0 M_s$, ω_0 is the Larmor pulsation given by $\omega_0 = \gamma\mu_0 H_i$ and the magnetic losses are modelled through the damping factor given by $\alpha = \frac{\gamma\Delta H}{2f}$ with ΔH the ferrite line width.

Therefore, μ and κ depend on the internal magnetic field in the ferrite H_i , the saturation magnetization M_s and the frequency f .

The effective permeability expressed by equation (3) is another important parameter that must be introduced for a clear understanding of this paper [26]:

$$\mu_{eff} = \frac{\mu^2 - \kappa^2}{\mu} \quad (3)$$

The Polder tensor elements and the effective permeability are used to define the antenna working zones already defined and studied in detail in [20]. In the example shown in Fig. 1, the Y36 ferrite, whose properties are summarized in Table I, is polarized with an internal field of 200 Oe. Plotting the real and imaginary parts of μ reveals the gyromagnetic resonance $f_0 = \gamma H_i$ (560 MHz in this example). Around this resonance frequency, the magnetic losses of the material are high. According to Fig. 1, four zones can be distinguished. The first (Zone 1) is called strong field area, where the device working frequency is below the gyromagnetic resonance. Zones 2, 3 and 4 are located in the weak field area. The Zone 2 is positioned between μ and μ_{eff} resonances, i.e. where the effective permeability is significantly higher than unity. The zone 3 is where the real part of the effective permeability is negative. The last zone (Zone 4) is where effective permeability becomes positive again.



Zone 1: Upstream of the gyromagnetic resonance
Gyromagnetic resonance
Zone 2: Between the resonances of μ and μ_{eff}
Zone 3: $\mu_{eff} < 0$
Zone 4: $\mu_{eff} > 0$

Fig. 1. Frequency evolution of μ and μ_{eff} for Y36 ferrite with an internal field H_i of 200 Oe.

TABLE I
FERRITE PROPERTIES

Ferrite	Y36
$4\pi M_s$	290 G
ΔH_{eff}	4 Oe
ΔH	25 Oe
ϵ_r	14
$\tan\delta$	0.0002

In [24] we have demonstrated an antenna operating in both Zones 1 and 4 to exhibit a multi-band antenna. In [20], an ultra-miniature working in Zone 2 has been developed. In the present

paper, we will focus the study on the last non-exploited zone, the Zone 3. This is an interesting area because it allows circular polarization to be obtained over a wide band.

As resonance frequencies of μ and μ_{eff} depend on the properties of the ferrite and the strength of the internal field, their choices have been adjusted so that the antenna's target operating frequencies (L1, L2 and E6) lie within Zone 3, where the real part of the effective permeability is negative.

III. PROPAGATING MODES IN A CYLINDRICAL FERRITE SUBSTRATE

In order to predict the operating frequency of the antenna as well as the geometric and magnetic specifications, a modal study of a cylindrical ferrite patch antenna is carried out before the modeling process with simulation tools. A cylindrical ferrite metallized in top and bottom faces could be modeled as a cylindrical resonant cavity as shown in Fig. 2 [26]. The cavity sides are assumed to be perfect magnetic walls and its upper and lower faces are considered perfect electrical walls.

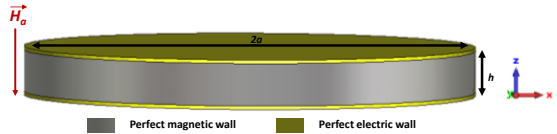


Fig. 2. Cylindrical ferrite patch antenna. \vec{H}_a is the applied magnetic field.

As already explained and detailed in [20], the application of the boundary conditions to the wave equation given by (4) leads to the determination of the working frequencies for $\mu_{eff} > 0$ by solving the equation (5) [26] and for $\mu_{eff} < 0$ by solving the equation (6) [20],[22].

$$\frac{\partial^2 E_z}{\partial \rho^2} + \frac{1}{\rho} \frac{\partial E_z}{\partial \rho} + \frac{1}{\rho^2} \frac{\partial^2 E_z}{\partial \phi^2} + k^2 E_z = 0 \quad (4)$$

$$J'_n(ka) \pm n \frac{k}{ka\mu} J_n(ka) = 0 \quad (5)$$

$$\frac{I'_n(ka)}{I_n(ka)} - \left(\frac{n}{ka} \right) \left(1 + \frac{\kappa}{\mu} \right) = 0 \quad (6)$$

With: $k = \omega \sqrt{\epsilon |\mu_{eff}|}$

Jn: Bessel functions

In: Modified Bessel functions

n represents the order of the Bessel function and also the variation of the mode along θ . Its sign defines the mode polarization: in positive signs ($n = +1; +2; \dots$) the wave is left-hand circularly polarized (LHCP) and in negative signs ($n = -1; -2; \dots$) is a right-hand circular polarization (RHCP). Applying a magnetic field in the negative z direction ($-\vec{H}_a$) as shown in Fig. 2, and plotting in Fig. 3 the evolution of the frequencies versus the internal magnetic field (H_i), it can be noticed the appearance of RHCP and LHCP modes on both sides of the

gyromagnetic resonance. The order of appearance of the LHCP or RHCP modes depends on the direction of the applied magnetic field \vec{H}_a . Reversing the internal field allows switching between RHCP and LHCP polarizations. For an internal magnetic field of 200 Oe applied in -z direction, an LHCP mode appears at 0.46 GHz in zone 1, and an RHCP mode at 0.79 GHz in Zone 2, at 1.27 GHz in RHCP corresponding to zone 3 and in zone 4 at 2 GHz in LHCP.

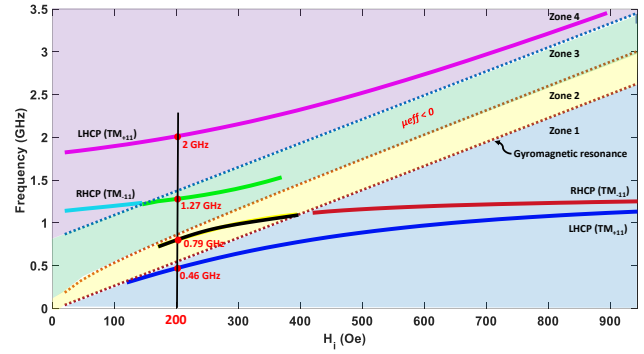


Fig. 3. Evolution of resonance frequencies as a function of the internal field applied in the -z direction. Resolution of propagation equations in the different study areas for modes order $n = \pm 1$.

A closer look at the existing modes in Zone 2 reveals a critical limitation to achieving good circular polarization over a wide frequency band. If we use the analytical calculation (Fig. 4) to trace the higher-order modes in the radial direction (a), we observe that these modes appear, in Zone 2, at frequencies very close to those of the fundamental mode. It is worth noting that in our specific design, the fundamental TM_{-11} mode appears at 0.79 GHz (generating RHCP), while a higher-order mode (TM_{+12}) appears at 0.83 GHz, corresponding to LHCP. These modes are very close to each other and have opposite circular polarizations. This explains the narrow axial ratio bandwidth in Zone 2, as the presence of this higher-order mode disrupts the desired RHCP operation.

In contrast, in the current Zone 3 ($\mu_{eff} < 0$), no higher-order radial modes are excited within the band of interest. This suggests that it is possible to achieve a good axial ratio over a wide frequency band.

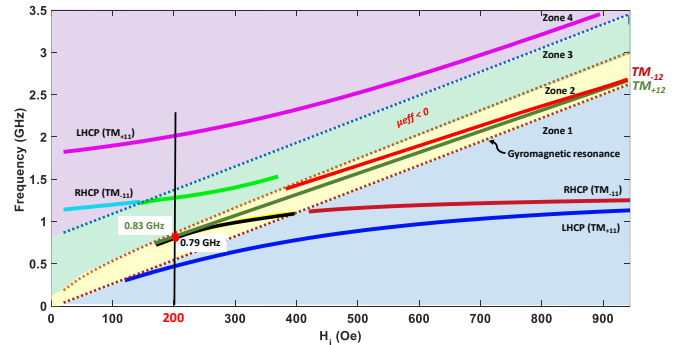


Fig. 4. An analytical study of the ferrite resonator taking into account higher-order radial modes.

Fig. 5 shows the evolution of E_z (normalized) component along the cavity of radius 16 mm for each frequency of the

modes appearing in the different zones for an internal magnetic field of 200 Oe applied along the $-z$ direction. For all modes, the field is maximum at the periphery of the ferrite and minimum at its center. This plot confirms that these are modes of order $n = \pm 1$, with different RHCP and LHCP polarizations.

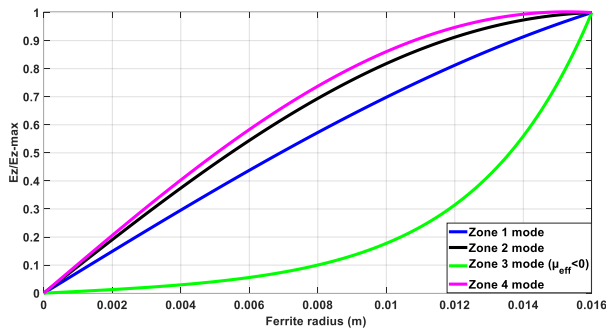


Fig. 5. Evolution of the normalized E_z component as a function of the cavity radius of the modes appearing in strong and weak fields for a $H_i = -200$ Oe.

Focusing on the zone where μ_{eff} is negative, a single polarization is observed with an RHCP mode appearing at 1.27 GHz. It exhibits a very strong (E_z) field at the edges of the cavity and undergoes a rapid evanescence as it moves away from the side walls. This suggests that it could only be excited if the feeding point is placed close to the resonator wall. This will be confirmed by electromagnetic simulation in the next section.

Therefore, to achieve a single polarization over a wide frequency band, it can be interesting to work in Zone 3. However, the configuration of the electric field and its amplitude suggest that there will be a challenge to excite this mode and match it in the case of an antenna. The next part will start from this theoretical analysis to retrieve the desired antenna properties through electromagnetic simulations.

IV. MODELING THE FERRITE PATCH ANTENNA

The first antenna design step considers the ferrite substrate with a homogeneous internal magnetic field while the second step uses magnetostatic (MS) and electromagnetic (EM) co-simulation considering the real field delivered by the magnet that will be used to bias and saturate the ferrite material.

A. Modeling the Ferrite Antenna with an Ideal Homogeneous Magnetic Field

1) Resonant Frequencies

Given the observations made in the previous section (strong field amplitude on the side wall of the resonator), we choose to excite the ferrite resonator using a microstrip line. This can be achieved by surrounding the ferrite resonator with a dielectric material. Alumina is chosen because it has a dielectric permittivity close to that of ferrite. The proposed device, depicted in Fig. 6, is composed of a cylindrical ferrite with a diameter of 34 mm and 3 mm of thickness, surrounded by a rectangular alumina (Al_2O_3) substrate ($\epsilon_r = 9.6$ and $\tan\delta = 2 \times 10^{-4}$) of 84 mm \times 94 mm. A circular metallic patch is placed on top of the ferrite with the same radius. This patch is edge-fed by a microstrip line and the lower metallization, over the entire surface of the substrate, acts as a ground plane. This antenna is

fed by a coaxial connector on the edge of the board. The first step in the modeling process of a ferrite antenna is to consider its response under a homogeneous bias magnetic field, along the whole ferrite substrate. A first simulation is done using an internal field in the ferrite $H_i = 200$ Oe applied along the $-z$ direction.

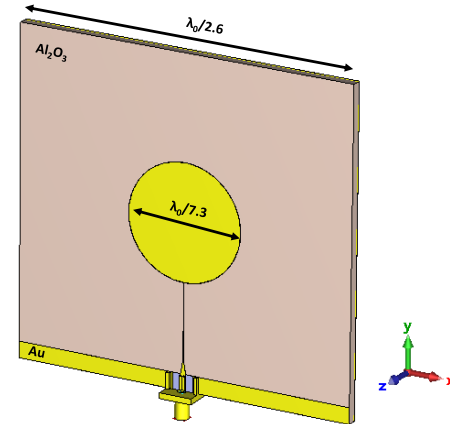


Fig. 6. Proposed antenna device topology.

The input impedance Z_{11} , presented in Fig. 7, has its reference plane at the ferrite-dielectric interface. It shows that a mode appears in the frequency band where the real part of the effective permeability is negative. Fig. 8 confirms that the excited mode is a TM_{+11} with a high intensity on the edge.

Fig. 9 shows the corresponding $|S_{11}|$ parameter and an operation around 1.27 GHz. As there is only one mode in this working zone (unlike the other zones that have already been published [20]), the RHCP polarization is not disturbed by the presence of other modes, resulting in an axial ratio (AR) of less than 3 dB over a frequency band wide enough to cover all the desired frequency bands L1, L2 and E6. In this case, the cavity mode is excited and centered around the E6 band (approximately 1.27 GHz), resulting in a good radiation efficiency, reaching up to 82 % at 1.28 GHz. This represents a promising solution for producing broadband or multiband antennas with the same circular polarization, on condition that they can be matched.

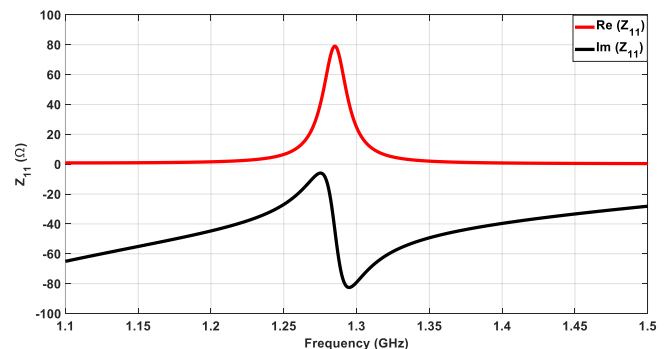


Fig. 7. Evolution of the real and imaginary part of the input impedance Z_{11} .

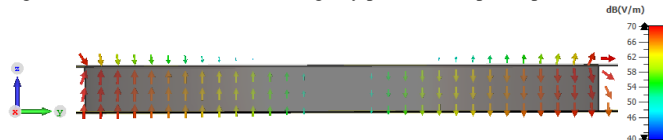


Fig. 8. Mapping of the E field at 1.27 GHz.

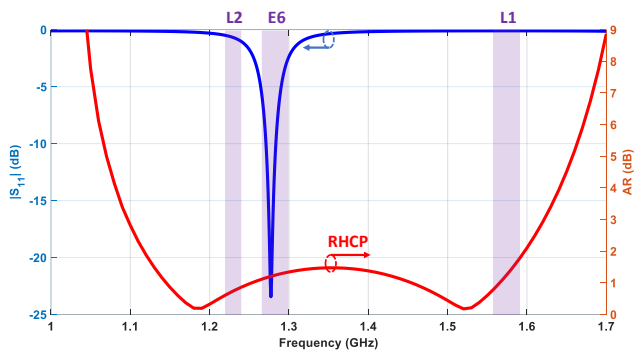


Fig. 9. $|S_{11}|$ and AR in EM simulation with an uniform H_i in the ferrite.

To obtain the antenna matching on the desired frequency bands, an ideal LC impedance matching circuit on the feeding line can be integrated to transform the previous Z_{11} (Fig. 7) to 50Ω on the L2 and E6 frequency bands (Fig. 10 (a)). Optimized values for the capacitance C1, and inductances L1 and L2 are 1.55 pF, 100 nH and 23 nH respectively. The corresponding $|S_{11}|$ parameter is plotted Fig. 10 (b). In order to avoid future losses linked to the integration of capacitances and inductances which could possibly disrupt and deteriorate the antenna radiation efficiency, an equivalent circuit was designed and optimized. This circuit is made up of a meander line as shown in Fig. 11 and is developed due to well-known studies in the literature [27], [28], [29].

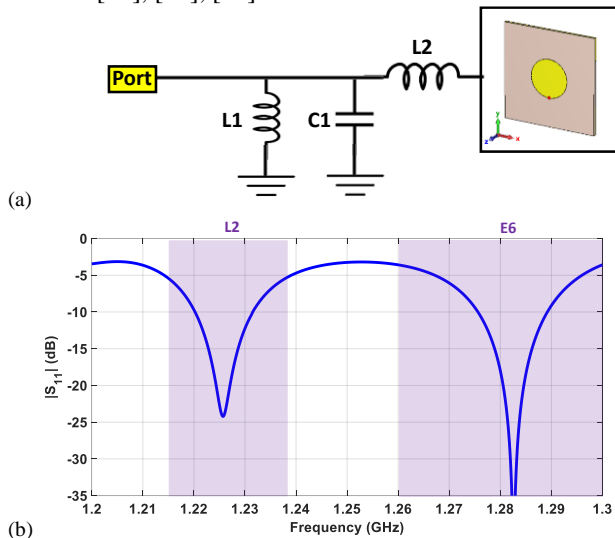


Fig. 10. (a) Antenna matching circuit to obtain the L2 and E6 bands. (b) The antenna $|S_{11}|$ parameter with a LC circuit integrated in the feeding line.

Etching a slot on the radiating element will allow matching the antenna on the L1 band (Fig. 11). The dimensions of the slot and matching circuit are $L_s = 16$ mm, $W_s = 0.5$ mm, $L_{g1} = 5.6$ mm, $W_1 = 0.3$ mm, $L_{g2} = 14.8$ mm, $W_2 = 0.15$ mm, $W_g = 0.25$ mm. The use of slots on patch antennas to increase bandwidth or enable multi-band operation has been extensively documented in the literature [30], [31], [32]. In this work, the slot is strategically etched near the edge of the radiating patch. As shown in Fig. 5, in the region where $\mu_{eff} < 0$, the E_z component is particularly strong along the cavity edge and decays toward the center. This field profile guided the shape of the slot arc and its peripheral placement. Its dimensions were optimized to excite a second resonance at the L1 band

frequency (~ 1.575 GHz), resulting in a dual-band RHCP response. Therefore, this will make it possible to achieve a tri-band antenna with the same RHCP in all frequency bands.

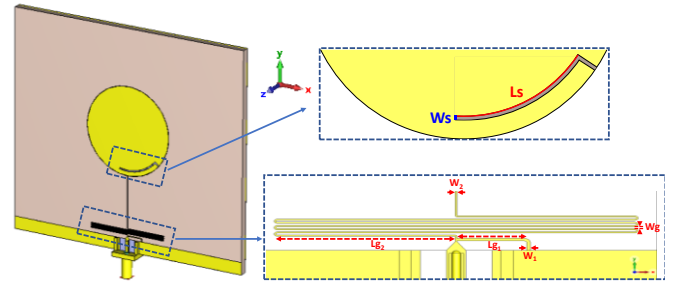


Fig. 11. Final antenna device configuration.

The $|S_{11}|$ and the axial ratio (AR) are plotted in Fig. 12. The antenna operates around 1.23 GHz, 1.282 GHz and 1.575 GHz with a good impedance matching on all frequency bands. The axial ratio plot highlights the good RHCP quality since the boresight AR remains under 3 dB on the device matching bands. These exceptional performance characteristics, however, come at the expense of radiation efficiency. The creation of these two additional resonances is enabled by the introduction of the meandered line which leads to a 20 % efficiency reduction compared to the previously mentioned peak efficiency of 82 %. In addition, the etched slot contributes to a further 12 % loss in efficiency on the lower frequency band.

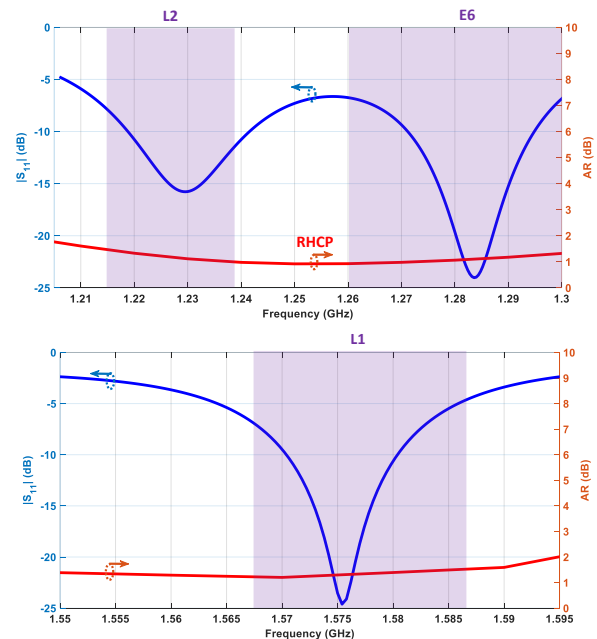


Fig. 12. The $|S_{11}|$ parameter and axial ratio (AR) versus the frequency under a uniform bias magnetic field of 200 Oe.

2) Radiation patterns

The circular polarization of the TM_{-11} excitation mode, obtained by the ferrite material integrated in the antenna device, can also be shown by the E-field distributions for different phases as presented in Fig. 13 at 1.23 GHz. Similar E-field distributions can be observed with other frequency bands.

The circularly polarized realized gains are exhibited in Fig. 14. From this illustration it appears that the device presents a conventional patch antenna radiation pattern which is maximum on the z- axis, the device main axis. The maximum realized gains are equal to 0 dBic, 1 dBic and 0.75 dBic for the L2, E6 and L1 bands respectively.

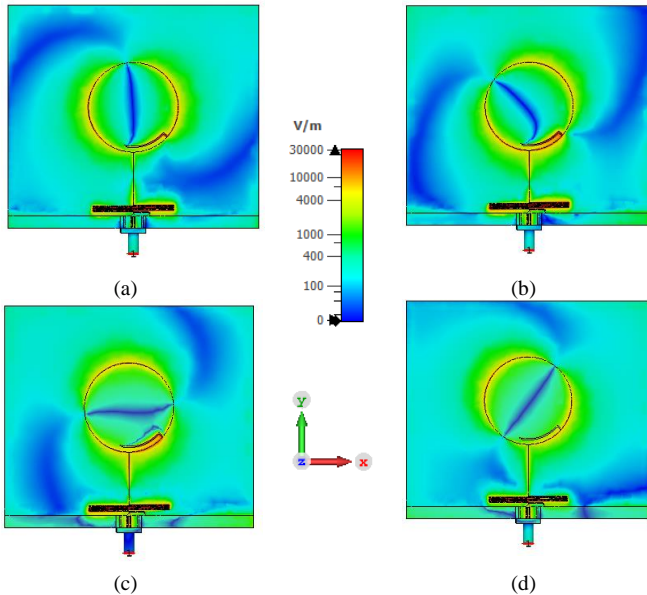


Fig. 13. E-field distributions of the ferrite antenna device at 1.23 GHz for (a) phase = 0°, (b) phase = 45°, (c) phase = 90° and (d) phase = 135°.

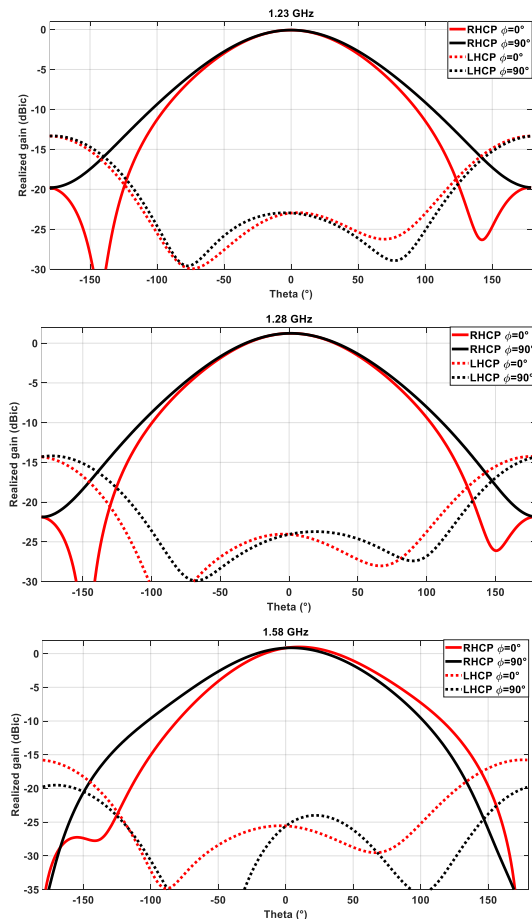


Fig. 14. Simulated radiation patterns for the proposed antenna in the three frequency bands, for an uniform H_z and for the cutting planes : $\phi = 0^\circ$ and $\phi = 90^\circ$.

3) Radiation efficiency analysis

The antenna radiates 30 % of the received power for all the matching bands, where the $|S_{11}|$ is under -10 dB. To find out why the radiation efficiency is low, we carried out further simulations.

One reason for the degraded efficiency of ferrite antennas is associated with the magnetic losses of the material [33]. However, the degradation in the efficiency of a miniature antenna is often linked to metal losses. As in the case presented here we are associating a ferrite material with miniaturization. Fig. 15 shows the contributions of each of the losses by plotting the evolution of the radiation efficiency as a function of the frequency for the different losses.

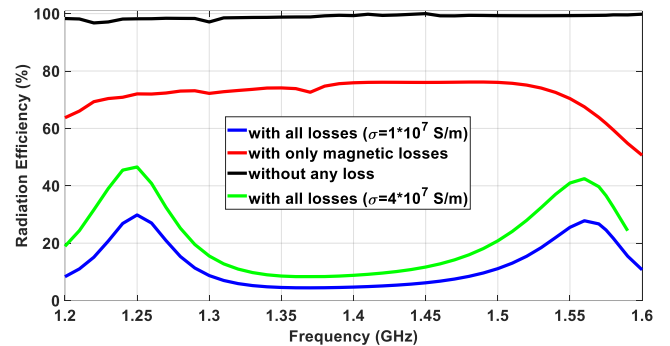


Fig. 15. Study of the influence of the conductivity in metal parts, the magnetic, metallic and dielectric losses on the ferrite antenna radiation efficiency.

The red plot in Fig. 15 considers only the magnetic losses of the device, that is to say, without the metallic and dielectric losses. The black plot of Fig. 15 is when the antenna has no loss and as expected a radiation efficiency of 100 % is obtained. In this case, a simplifying assumption considering the ferrite as an isotropic magneto-dielectric material has been made. The magnetic losses of the material were set to 0 as well as its dielectric loss tangent. Moreover, metallic plates constituting the patch, lines and ground plane were replaced with perfect electrical conductors (PEC).

The blue and green curves consider all the losses and also show the influence of the metal's conductivity value. Therefore, metallic losses cause more than 40 % reduction in efficiency in the worst case, i.e. when the metallic conductivity is $1 \cdot 10^7$ S/m. Indeed, electrical currents flowing through the meander line can cause part of the RF signal power to be lost in the metal. As shown in Fig. 13, a high concentration of E-field existing around this feeding line affects also the efficiency of the antenna. The low conductivity of $1 \cdot 10^7$ S/m for metallic parts in the device has been considered since this value corresponds to the real conductivity of the metallization that will be used in the manufacturing process of the device in our laboratory's clean room. This variation of conductivity adds a loss of 15 % in the efficiency of the antenna.

Therefore, we can conclude that working in the zone with the real part of μ_{eff} is negative allows to improve the AR bandwidth of an antenna with a radiation efficiency that could be improved by the development of optimized manufacturing process.

B. Ferrite Antenna Behavior under an Inhomogeneous Internal Magnetic Field

In the real case (for the realization of the experimental device),

this kind of ferrite substrate is biased by permanent magnets to be considered in simulation. Before simulating the antenna behavior in this practical case, it is necessary to define the geometrical and magnetic characteristics of the magnets to evaluate the needed DC biasing field for the ferrite. For this reason, a magnetostatic study must be performed.

The chosen magnet shown in Fig. 16 is a Samarium Cobalt (SmCo5), with a $B_r = 0.88$ T, located under the ground plane, with a diameter of 60 mm and a thickness of 3.2 mm. To improve the field homogeneity, a steel plate was added between the ground plane and the magnet. Whether the homogeneity of the internal static magnetic field H_i on the ferrite can be improved even more, by using a second magnet placed on top, as is commonly found in the literature [17], [20], [24], here the etched slot on the patch for the L1 band, prevents this type of configuration with two magnets. Consequently, H_i in the ferrite will be less uniform than commonly used models.

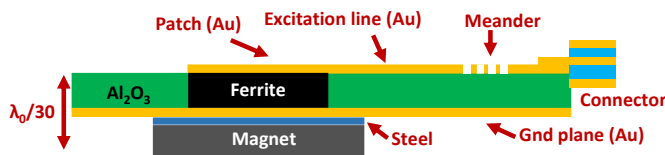


Fig. 16. Side cut of the simulated antenna final design considering a non-homogeneous internal magnetic field provided by permanent magnets.

Considering all the antenna components, including the magnet and steel plate, the total dimension of the device antenna is $\frac{\lambda_0}{2.9} \times \frac{\lambda_0}{2.6} \times \frac{\lambda_0}{30}$ (ground plane length \times width \times total height) at 1.23 GHz.

Magnetostatic and electromagnetic simulations are combined to estimate the antenna's performance, considering the actual H_i values obtained with the magnets. These MS-EM co-simulation results, in terms of $|S_{11}|$ parameter and AR in the boresight direction ($\varphi = 0^\circ$ and $\theta = 0^\circ$), are plotted in Fig. 17 as a function of frequency, with H_i oriented along the negative z axis.

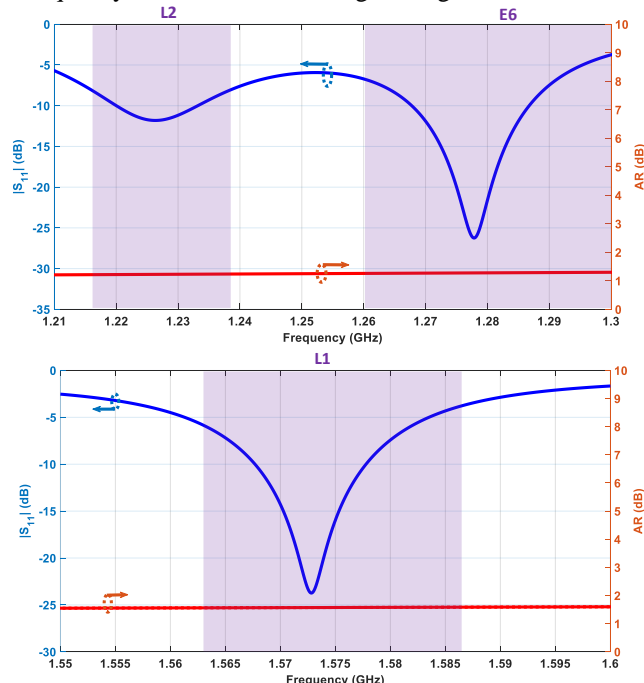


Fig. 17. The $|S_{11}|$ parameters and the AR of MS-EM co-simulation for a non-uniform bias magnetic field.

The antenna has an RHCP in the three operating bands (L1, L2 and E6), with an AR < 3 dB which covers all of the matching frequency bands of the antenna.

The slight differences between ideal and real case studies, in terms of AR and $|S_{11}|$ parameter behavior and frequency shifts are mostly due to the H_i inhomogeneity. In the zone where $\mu_{eff} < 0$, a slight variation of H_i leads to a variation of μ_{eff} (Fig. 1) and thus of the antenna performances. These differences (between ideal and real case studies) are more visible in terms of radiation pattern (gain and efficiency). The realized gain is about -2.3 dBi, 0.19 dBi and 0.2 dBi at the central frequencies for the L2, E6 and L1 bands respectively.

In summary, from this MS-EM co-simulation analysis, the antenna performances of the ideal case study could be basically retrieved by properly adjusting the magnetic biasing field from the magnets. The next step consists in validating the simulated results through a prototype measurement.

V. REALIZATION OF THE PROTOTYPE AND MEASUREMENT RESULTS

After the simulations, performance validation will be carried out by measuring a prototype. A bare alumina - ferrite substrate was metallized on both sides using microfabrication techniques available in the clean room of the XLIM Research Institute. The metallic parts of the antenna (main patch, feeding line and ground plane) were fabricated using a Ti/Au (30/300 nm) layer obtained by electron-beam evaporation, completed by an electrolysis to achieve a gold layer of 15 μm thick. The etching of the upper face of the antenna (main patch and feeding line) was carried out by an LPKF laser machine. Then the SMA connector is fixed by a silver conductive glue. For assembling the antenna elements, the steel plate and the magnet were aligned with the ground plane and ferrite through a Rohacell support (Fig. 18).



Fig. 18. The bare ferrite and alumina substrate, the fabricated antenna after metallization and laser etching and the antenna mounted inside the Rohacell support.

The measurements of the proposed antenna were carried out within the CISTEME measurement platform using an SG 24 Stargate, as shown in Fig. 19. The radiation pattern of the antenna under test (AUT) was measured in a transmit configuration using

a dedicated Rohacell support to minimize external perturbations and measurement artifacts.



Fig. 19. SG 24 Stargate measurement setup used for the characterization of the fabricated antenna (antenna under test – AUT).

The co-simulated and measured $|S_{11}|$ parameters and the boresight AR as a function of frequency are plotted in Fig. 20. The three operating bands are around 1.225 GHz, 1.279 GHz and 1.573 GHz respectively with a good agreement between the measured and simulated parameters. The boresight AR of the antenna is of the order of 1.2 dB to 1.4 dB on the L2 and E6 bands and below 1.6 dB on the upper band L1.

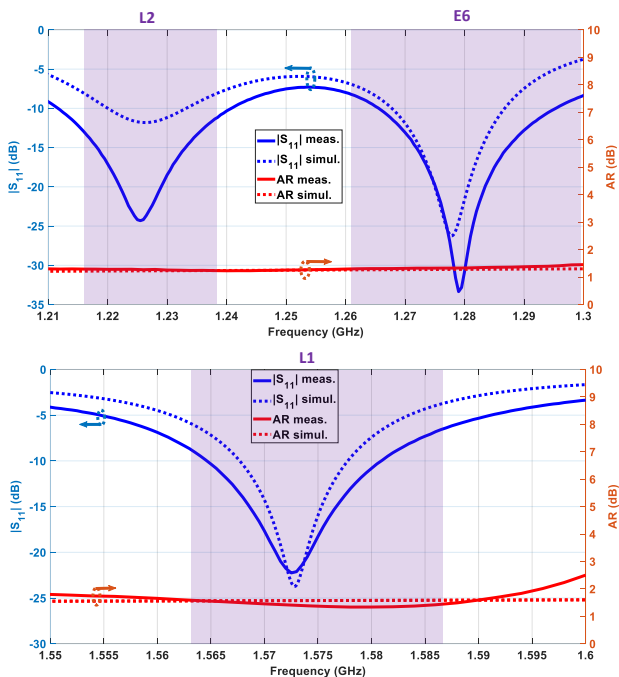


Fig. 20. Measurement results and MS-EM co-simulation of $|S_{11}|$ parameters and AR for the three operating frequencies.

Fig. 21 shows the measured AR of the right polarization (main polarization) at the frequencies 1.225 GHz, 1.279 GHz and 1.573 GHz for different cutting planes ($\phi = 0^\circ$, $\phi = 45^\circ$, $\phi = 90^\circ$ and $\phi = 135^\circ$). These measurement results demonstrate the good radiation in right hand circular polarization of the fabricated device. The antenna reveals an $AR < 3$ dB with an angular

aperture in the theta plane between -100° and 110° for the frequency bands L2 and E6 in the different ϕ cutting planes. Even in the worst case for the L1 band, the angular aperture in the theta plane remains between -68° and 75° with an $AR < 3$ dB.

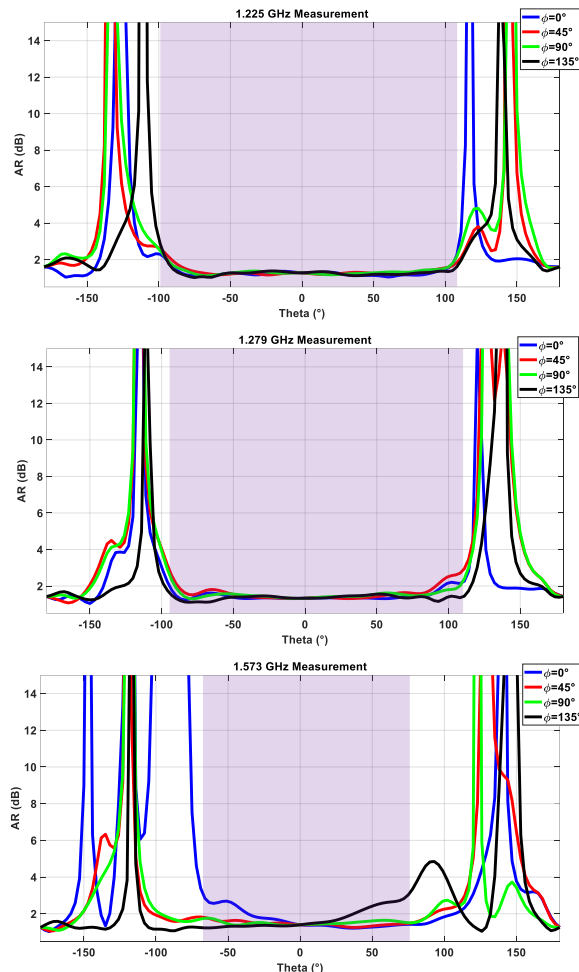


Fig. 21. Axial ratio of the right hand circular polarization (RHCP) at 1.225 GHz, 1.279 GHz and 1.573 GHz for different Phi cutting planes.

To provide a comprehensive evaluation of the antenna's performance, the measured boresight realized gain is plotted as a function of frequency (Fig. 22). For clarity, the measured $|S_{11}|$ parameter is also included in the same plot. The measured results demonstrate realized gains ranging from -4.1 dBic to -1.8 dBic in the L2 band, from -4.1 dBic to 1 dBic in the E6 band, and from -1.8 dBic to 1 dBic in the L1 band. Across all frequency bands, the minimum gain of -4.1 dBic occurs at the lower edge of the L2 band and at the peak frequency of the E6 band. The measured radiation efficiency of the antenna exhibits a trend consistent with that of the realized gain, as illustrated in Fig. 22.

The efficiency reaches peak values of 28 % in the L2 and E6 bands, and 26 % in the L1 band. These efficiency values are quite close to those obtained in the EM simulation (blue plot of Fig. 15). For a better estimation of the concordance between measurement and the MS-EM co-simulation antenna behavior, Table II summarizes the performances obtained in terms of gain, radiation efficiency and boresight AR on the central frequency of $|S_{11}|$ parameters for the three bands.

From this comparative study, even if ensuring a perfect homogeneity of the H_i in ferrite antennas is a real challenge, it

has been possible to successfully align simulation and measurements. Due to the prototype realization and despite the difficulties to reproduce in simulation the real field provided by the magnets, the concept of a tri-band antenna operating in a $\mu_{eff} < 0$ zone with an RHCP wave is validated for GPS and Galileo applications.

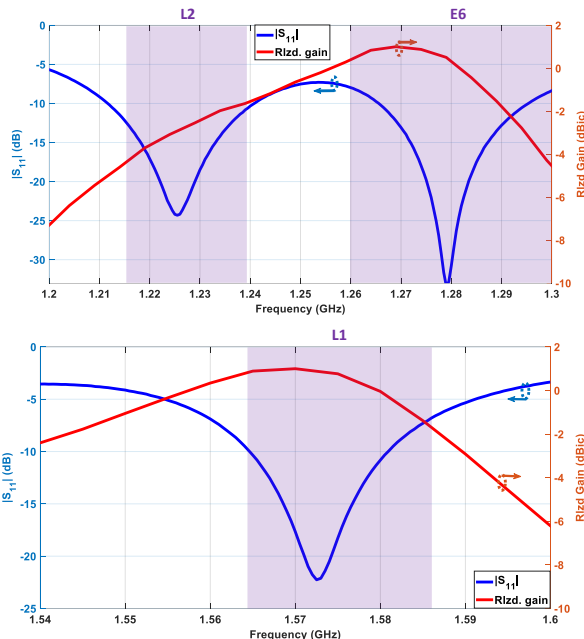


Fig. 22. Measured realized gain of the antenna as a function of frequency.

TABLE II
SUMMARY OF THE MEASURED PERFORMANCES OF THE FABRICATED ANTENNA DEVICE

Frequency	1.225 GHz	1.279 GHz	1.573 GHz
AR ($\varphi = 0^\circ, \theta = 0^\circ$)	1.26 dB	1.33 dB	1.4 dB
Radiation efficiency	10 %	24 %	24 %
Realized gain	-3 dBic	0.2 dBic	0.9 dBic
Simulated realized gain	-2.3 dBic	0.19 dBic	0.2 dBic

VI. COMPARISON WITH THE LITERATURE

The performances of some existing antennas in the literature operating in the $\mu_{eff} < 0$ zone and multiband antennas for GNSS applications are compared in the Table III with the ones presented in this paper. It is worth noting that some of the ferrite antennas listed in Table III ([21], [22], [23]) are only simulated under the ideal condition of a uniform magnetic field in the ferrite, without the use of biasing magnets, and lack experimental validation.

The listed dimensions in the third column include the ground plane which contributes to the radiation performances of the antenna like an improvement of the realized gain or the impedance bandwidth. This work offers a more compact device compared to conventional antennas (without ferrite substrate) for the same GNSS applications ([34], [35], [36]) or to other ferrite antennas operating in the $\mu_{eff} < 0$ zone [21], [22]. In cases where the impedance bandwidths are wider than this work, the devices use low permittivity and much bulkier substrates [34] or several radiating elements [22], which could also explain larger gain values. It should also be noted that the measured 3-dB AR

beamwidth is wider in this work than for other ferrite devices in the $\mu_{eff} < 0$ zone ([21], [22], [23]).

In [24], a different approach is adopted by exploiting the eigenmodes of a cavity filled with a dispersive ferrite material. These eigenmodes reappear at multiple frequencies, enabling multi-band circularly polarized operation through direct excitation with a coaxial probe. The efficiency and gain measurements in [24] are referenced at the output of the coaxial line, just before the antenna input, ensuring direct excitation and good matching at cavity resonances, resulting in higher measured realized gains. While this method leads to efficient and multi-band operation, the resonant frequencies are inherently coupled through the cavity geometry and material dispersion, limiting the ability to independently target closely spaced GNSS bands such as L1, L2, and E6. Furthermore, this approach results in the simultaneous presence of both RHCP and LHCP polarizations, which is not acceptable for GNSS applications that require consistent and pure RHCP across all operating bands.

VII. CONCLUSION

The present article exploits the potential of ferrite material to produce a compact multiband antenna for GNSS applications, with a small footprint, radiating a right-handed circular polarization over three frequency bands with a single feed point and a single ferrite substrate.

Based on a theoretical approach and MS-EM co-simulations, we have demonstrated that working in the zone where the real part of the effective permeability is negative provides a wide frequency band of an AR lower than 3 dB. The antenna was manufactured and the measured performances demonstrate proper operation of the device on this ferrite working Zone ($\mu_{eff} < 0$) rarely studied in the literature. In fact, this zone is often neglected since a slight variation of the magnetic field leads to a variation of the effective permeability which may affect the antenna response.

All the device development has been detailed, starting with a prediction of the antenna performances in the ideal case, i.e. considering a homogeneous internal magnetic field. Then, the ferrite substrate was biased by a permanent magnet and a magnetostatic study was carried out to estimate the magnetic field produced by this magnet and the non-homogeneous internal magnetic field in the ferrite. Finally, a prototype has been realized and the comparison of the measured and simulated results showed a good agreement validating the concept of a tri-band antenna for the first time with a ferrite substrate with the same circular polarization (RHCP) on the three operating frequency bands.

ACKNOWLEDGMENT

This work was supported and funded by the French Defence Innovation Agency (AID) and the French National Research Agency (ANR) in the framework of the CONTACT project (ANR-20-ASTR-0010).

This work was carried out as part of the INOGYRO joint laboratory between the SME Inoveos and the XLIM Research Institut (<https://inogyro.xlim.fr/>). The measurements were carried out within the CISTEME measurement platform using a SG 24 Stargate (<https://cisteme.net/>).

TABLE III
COMPARISON WITH CP ANTENNAS IN THE PREVIOUS LITERATURE

Reference	Operating frequency (GHz)	Dimension	3-dB AR Beamwidth (°)	Maximum realized gain on the bandwidth (dBic)			Measured results	Type of polarization	Number of patches
[21]	3.9	$\frac{\lambda_0}{0.9} \times \frac{\lambda_0}{0.9} \times \frac{\lambda_0}{72}$	200	5			No	LHCP	1
[22]	4.22	$\frac{\lambda_0}{1.4} \times \frac{\lambda_0}{1.4} \times \frac{\lambda_0}{40}$	90	7			No	LHCP	1
[23]	4.1	$\frac{\lambda_0}{2.6} \times \frac{\lambda_0}{2.6} \times \frac{\lambda_0}{44}$	180	7.9			No	LHCP	6
[24]	3.3, 3.9, 7.4	$\frac{\lambda_0}{4.5} \times \frac{\lambda_0}{4.5} \times \frac{\lambda_0}{6.9}$	NA	1.8	2.6	3.7	Yes	RHCP, LHCP, RHCP	1
[34]	1.165-1.19, 1.195-1.24, 1.37-1.395, 1.565-1.585	$\frac{\lambda_0}{1.2} \times \frac{\lambda_0}{1.2} \times \frac{\lambda_0}{4.4}$	135	7.7 (L2)	NA (E6)	7.94 (L1)	Yes	RHCP (all frequencies)	NA
[35]	1.15-1.29; 1.5-1.615	$\frac{\lambda_0}{3.4} \times \frac{\lambda_0}{4.4}$	120	3 (L2)	3 (E6)	2 (L1)	Yes	RHCP (all frequencies)	NA
[36]	1.227; 1.525-1.61	$\frac{\lambda_0}{2} \times \frac{\lambda_0}{3} \times \frac{\lambda_0}{8.8}$	AR > 3dB	3 (L2)	NA (E6)	2 (L1)	Yes	RHCP (all frequencies)	NA
This work	1.225, 1.279, 1.573	$\frac{\lambda_0}{2.6} \times \frac{\lambda_0}{2.9} \times \frac{\lambda_0}{30}$	210	-1.8 (L2)	1 (E6)	1 (L1)	Yes	RHCP (all frequencies)	1

Part of the work has been performed with the means of the technological platforms Platinom at the XLIM Research Institute (www.unilim.fr/platinom), supported by the European regional development foundation and the French government with the New Aquitaine region (FEDER-PILIM 2015-2020).

The authors acknowledge the use of OpenAI tools to partially generate Fig. 19 for illustrative purposes. The AI system was not used to generate or modify any experimental results or scientific data.

REFERENCES

- [1] J. L. Valdes, L. Huitema, E. Arnaud, D. Passerieux, and A. Crunteanu, "A Polarization Reconfigurable Patch Antenna in the Millimeter-Waves Domain Using Optical Control of Phase Change Materials," *IEEE Open J. Antennas Propag.*, vol. 1, pp. 224–232, 2020, doi: 10.1109/OJAP.2020.2996767.
- [2] E. Aloni and R. Kastner, "Analysis of a dual circularly polarized microstrip antenna fed by crossed slots," *IEEE Trans. Antennas Propag.*, vol. 42, no. 8, pp. 1053–1058, Aug. 1994, doi: 10.1109/8.309996.
- [3] E. Herth, N. Rolland, and T. Lasri, "Circularly Polarized Millimeter-Wave Antenna Using 0-Level Packaging," *Antennas Wirel. Propag. Lett.*, vol. 9, pp. 934–937, 2010, doi: 10.1109/LAWP.2010.2080310.
- [4] H. Wong, K. K. So, K. B. Ng, K. M. Luk, C. H. Chan, and Q. Xue, "Virtually Shorted Patch Antenna for Circular Polarization," *Antennas Wirel. Propag. Lett.*, vol. 9, pp. 1213–1216, 2010, doi: 10.1109/LAWP.2010.2100361.
- [5] K. Y. Lam, K.-M. Luk, Kai Fong Lee, H. Wong, and K. B. Ng, "Small Circularly Polarized U-Slot Wideband Patch Antenna," *Antennas Wirel. Propag. Lett.*, vol. 10, pp. 87–90, 2011, doi: 10.1109/LAWP.2011.2110631.
- [6] K.-F. Tong and T.-P. Wong, "Circularly Polarized U-Slot Antenna," *IEEE Trans. Antennas Propag.*, vol. 55, no. 8, pp. 2382–2385, Aug. 2007, doi: 10.1109/TAP.2007.901930.
- [7] Jui-HanLu, Chia-LuanTang, and Kin-LuWong, "Circular polarisation design of a single-feed equilateral-triangular microstrip antenna," *Electronics Letters*, pp. 1989–1990, Oct. 15, 1998.
- [8] Y. J. Sung and Y.-S. Kim, "Circular polarised microstrip patch antennas for broadband and dual-band operation," *Electron. Lett.*, vol. 40, no. 9, p. 520, 2004, doi: 10.1049/el:20040379.
- [9] Sung Min Kim, Yong Hee Kim, and Woon Geun Yang, "Design and implementation of dual-band circular polarization square patch antenna for GPS and DMB," in *2006 IEEE Antennas and Propagation Society International Symposium*, Albuquerque, NM, USA: IEEE, 2006, pp. 2653–2656. doi: 10.1109/APS.2006.1711147.
- [10] X. L. Bao and M. J. Ammann, "Printed circularly polarised antenna with ultra-wide axial-ratio bandwidth," *IET Microw. Antennas Propag.*, vol. 5, no. 9, p. 1089, 2011, doi: 10.1049/iet-map.2010.0493.
- [11] M. Koubeissi, E. Arnaud, M. Thevenot, T. Monediere, E. Peragin, and H. Diez, "Wide aperture circularly polarized antenna for small telemetry satellites," *Int. J. Microw. Wireless Technol.*, vol. 4, no. 6, pp. 623–628, Dec. 2012, doi: 10.1017/S1759078712000608.
- [12] L. Rudant, L. Batel, A. Clemente, and C. Delaveaud, "New Approach in Antenna Design Automation Applied to a Dual-Band GNSS Micro-Array," in *2021 15th European Conference on Antennas and Propagation (EuCAP)*, Dusseldorf, Germany: IEEE, Mar. 2021, pp. 1–5. doi: 10.23919/EuCAP51087.2021.9411019.
- [13] E. Andreou, T. Zervos, A. A. Alexandridis, and G. Fikioris, "Magnetodielectric Materials in Antenna Design: Exploring the Potentials for Reconfigurability," *IEEE Antennas Propag. Mag.*, vol. 61, no. 1, pp. 29–40, Feb. 2019, doi: 10.1109/MAP.2018.2883029.
- [14] E. Andreou *et al.*, "Reconfigurable proximity coupled patch antenna using magnetic bias," in *2014 Loughborough Antennas and Propagation Conference (LAPC)*, Loughborough, Leicestershire, United Kingdom: IEEE, Nov. 2014, pp. 376–380. doi: 10.1109/LAPC.2014.6996401.
- [15] T. Zervos, A. A. Alexandridis, F. Lazarakis, and K. Dangakis, "Patch antenna with polarization agility using ferrimagnetic materials," in *2009 Loughborough Antennas & Propagation Conference*, Loughborough: IEEE, Nov. 2009, pp. 541–544. doi: 10.1109/LAPC.2009.5352431.
- [16] M. Sigalov, R. Shavit, and E. O. Kamenetskii, "Dual band circular polarized patch antenna using small ferrite disks," in *2008 IEEE 25th Convention of Electrical and Electronics Engineers in Israel*, Eilat, Israel: IEEE, Mar. 2008, pp. 523–527. doi: 10.1109/EEEL.2008.4736584.
- [17] E. Arnaud, L. Huitema, R. Chantalat, A. Bellion, and T. Monediere, "Miniaturization of a Circular Polarized Antenna using Ferrite

Materials,” in *12th European Conference on Antennas and Propagation (EuCAP 2018)*, London, UK: Institution of Engineering and Technology, 2018, p. 558 (5 pp.)-558 (5 pp.). doi: 10.1049/cp.2018.0917.

[18] S. Jemmel, T. Monediere, E. Arnaud, and L. Huitema, “Design of a Miniature Circularly Polarized Antenna Operating in Three Frequency Bands Using a Polarized Ferrite Material,” *IEEE Trans. Antennas Propagat.*, vol. 69, no. 8, pp. 4304–4312, Aug. 2021, doi: 10.1109/TAP.2020.3045756.

[19] A. A. Mavridis, G. A. Kyriacou, and J. N. Sahalos, “ON THE DESIGN OF PATCH ANTENNAS TUNED BY TRANSVERSELY MAGNETIZED LOSSY FERRITE INCLUDING A NOVEL RESONATING MODE,” *PIER*, vol. 62, pp. 165–192, 2006, doi: 10.2528/PIER06041301.

[20] S. Jemmel, T. Monediere, E. Arnaud, and L. Huitema, “Ultra-Miniature and Circularly Polarized Ferrite Patch Antenna,” *IEEE Trans. Antennas Propagat.*, vol. 71, no. 8, pp. 6435–6443, Aug. 2023, doi: 10.1109/TAP.2023.3284166.

[21] M. B. Heydari and A. Ahmadvand, “A novel analytical model for a circularly-polarized, ferrite-based slot antenna by solving an integral equation for the electric field on the circular slot,” *Waves in Random and Complex Media*, vol. 32, no. 2, pp. 509–528, Mar. 2022, doi: 10.1080/17455030.2020.1782510.

[22] J. Ghalibafan, B. Rejaei, and N. Komjani, “A Circularly Polarized Antenna Based on the Unidirectional Resonant Modes of a Ferrite Disk,” *IEEE Trans. Magn.*, vol. 50, no. 3, pp. 88–95, Mar. 2014, doi: 10.1109/TMAG.2013.2283655.

[23] M. Mashhadi, B. Rejaei, N. Komjani, and J. Ghalibafan, “Analysis of Wideband Circularly Polarized Ferrite-Loaded Antenna Based on Unidirectional Resonant Modes,” *IEEE Trans. Magn.*, vol. 53, no. 9, pp. 1–8, Sep. 2017, doi: 10.1109/TMAG.2017.2708026.

[24] S. Jemmel, T. Monediere, E. Arnaud, and L. Huitema, “Design of a Miniature Circularly Polarized Antenna Operating in Three Frequency Bands Using a Polarized Ferrite Material,” *IEEE Trans. Antennas Propagat.*, vol. 69, no. 8, pp. 4304–4312, Aug. 2021, doi: 10.1109/TAP.2020.3045756.

[25] D. Polder, “On the theory of ferromagnetic resonance,” *Physica*, vol. 15, no. 1–2, pp. 253–255, Apr. 1949, doi: 10.1016/0031-8914(49)90051-8.

[26] D. M. Pozar, “Radiation and scattering characteristics of microstrip antennas on normally biased ferrite substrates,” *IEEE Trans. Antennas Propagat.*, vol. 40, no. 9, pp. 1084–1092, Sep. 1992, doi: 10.1109/8.166534.

[27] S.-M. Yang and C.-H. Huang, “An Inductor Model for Analyzing the Performance of Printed Meander Line Antennas in Smart Structures,” *JEMAA*, vol. 06, no. 09, pp. 244–252, 2014, doi: 10.4236/jemaa.2014.69025.

[28] P. M. Sihombing, H. A. Samosir, L. T. Hutabarat, M. W. Sitopu, J. Margolang, and J. Hidayat, “Microstrip Antenna Design Using Meander Line Technique for Communication between Pilot and Air Traffic Controller in VHF A/G Band,” in *2020 4rd International Conference on Electrical, Telecommunication and Computer Engineering (ELTICOM)*, Medan, Indonesia: IEEE, Sep. 2020, pp. 111–114. doi: 10.1109/ELTICOM50775.2020.9230499.

[29] X. Hu, Y. Liu, and Y. Yang, “Miniaturized 3-bit frequency-reconfigurable monopole antenna with a meander line,” *Electronics Letters*, vol. 59, no. 23, p. e13030, Dec. 2023, doi: 10.1049/ell2.13030.

[30] P. Mohana Sunthari and R. Veeramani, “Multiband microstrip patch antenna for 5G wireless applications using MIMO techniques,” presented at the 2017 First International Conference on Recent Advances in Aerospace Engineering (ICRAAE), Coimbatore, India, Mar. 2017. doi: 10.1109/ICRAAE.2017.8297241.

[31] Lalbabu Prasad, Ramesh Boddu, K. S. R. Kumar, and K. P. Vinay, “Design and Implementation of Multiband Microstrip Patch Antenna for Wireless Applications,” *Advanced Electromagnetics*, vol. 7, no. 3, Aug. 2018, doi: 10.7716/aem.v7i3.646.

[32] P. Bhartia, Inder Bahl, R. Garg, and A. Ittipiboon, *Microstrip Antenna Design Book*. Artech House Publishers, 2000.

[33] E. Andreou *et al.*, “Magneto-dielectric substrate influence on the efficiency of a reconfigurable patch antenna,” in *2017 International Workshop on Antenna Technology: Small Antennas, Innovative Structures, and Applications (iWAT)*, Athens, Greece: IEEE, 2017, pp. 191–194. doi: 10.1109/IWAT.2017.7915355.

[34] S. X. Ta, H. Choo, I. Park, and R. W. Ziolkowski, “Multi-Band, Wide-Beam, Circularly Polarized, Crossed, Asymmetrically Barbed Dipole

Antennas for GPS Applications,” *IEEE Trans. Antennas Propagat.*, vol. 61, no. 11, pp. 5771–5775, Nov. 2013, doi: 10.1109/TAP.2013.2277915.

[35] “Antenne de précision multi-GNSS PCTEL GNSS-L125-TNC.” [Online]. Available: https://canalgeomatics.com/fr/product/pctel-gnss-l125-tnc-multi-gnss-precision-antenna/?utm_source=chatgpt.com

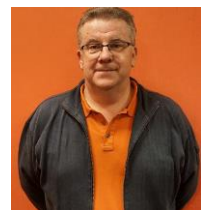
[36] “Antenne GNSS multibande PCTEL GPS-LB12GL-MAG.” [Online]. Available: https://canalgeomatics.com/fr/product/pctel-gps-lb12gl-mag-multiband-gnss-antenna/?utm_source=chatgpt.com



Jehison Leon Valdes received the M.S. and Ph.D. degrees in telecommunications high frequencies and optics from the University of Limoges, Limoges, France, in 2017 and 2020, respectively. He is currently a Post-Doctoral Research Fellow within the Antennas and Signals Team of the RF systems axis of the XLIM Research Institute. His research interests include circularly polarized, reconfigurable, miniature and multiband antennas using ferrite materials and phase change materials.



Thierry Monediere received the Ph.D. degree from the IRCOM Laboratory, University of Limoges, Limoges, France, in 1990. He is currently a Professor with the Antennas and Signals Team, XLIM Research Laboratory, University of Limoges. He develops his research activities in this laboratory and works on multifunction antennas, miniature antennas, antenna arrays, and also active antennas. He also studies gyromagnetic devices as ferrite circulators or isolators.



Eric Arnaud received the Diplôme D’Études Supérieures Spécialisées (DESS) and Ph.D. degrees in electronics and telecommunication from the University of Limoges, Limoges, France, in 1994 and 2010, respectively. He did his Ph.D. on circularly polarized EBG antenna. From 1996 to 2001, he has been in charge of the Microwave part of Free-Electron Laser (L.U.R.E). Since 2001, he has been in charge of XLIM Laboratory’s Antenna Test Range. He participated in several research projects related to the design, development, and characterization of antennas. His research interests are mainly in the fields of circularly polarized antenna, agile electromagnetic band gap matrix antenna, and isoflux pattern antenna.



Sarra Jemmel received the Ph.D. degree in high-frequency electronics from the University of Limoges, Limoges, France, in 2021. From 2021 to 2022, she was a Post-Doctoral Researcher with the joint laboratory INOgyro, Limoges, which associates the research institution XLIM with the SME INOVEOS. Currently, she is a Research and Development Engineer with Exens-Solutions, Les Ulis, France (previously Cobham Microwave). Her research focuses on circularly polarized, miniature, and multiband antennas using ferrite materials.



Laure Huitema received the M.S. and Ph.D. degrees in telecommunications high frequencies and optics from the University of Limoges, Limoges, France, in 2008 and 2011, respectively. From 2011 to 2012, she was a Post-Doctoral Research Fellow with the Atomic Energy Commission (CEA), Laboratory of Electronics and Information Technology (LETI), Grenoble, France. She is currently an Associate Professor with the Antennas and Signals Team within the RF systems axis of the XLIM Research Institute, University of Limoges.

More recently, she has been working on the integration of new components based on innovative materials for their integration into antennas and was the Project Leader of a European H2020 Project called MASTERS. Since 2019, she has been the Director of the joint laboratory INOGYRO, Limoges, which groups together the XLIM Laboratory and the company INOVEOS. Her research interests include reconfigurable antennas, dielectric resonator antennas, miniature antennas, multiband antennas, and circulators. Dr. Huitema received the Best Student Paper Award by IEEE International Workshop on Antenna Technology (IWAT) in 2010 and Journées de Caractérisation Microondes et Matériaux (JCMM) in 2010 conference. In 2020, she was also awarded the bronze medal from Centre national de la recherche scientifique (CNRS) (the French National Center for Scientific Research).